Cryogenics 123 (2022) 103441

Contents lists available at ScienceDirect

Cryogenics

journal homepage: www.elsevier.com/locate/cryogenics

Performance comparison of sorption compressors for methane using metal-organic frameworks and activated carbon as adsorbents

Lingxiao Qin [a], Haishan Cao [a,*], Junming Li [a], Yingzhe Wu [b], Marcel ter Brake [c]

[a] Key Laboratory for Thermal Science and Power Engineering of Ministry of Education, Tsinghua University, Beijing 100084, China
[b] Shanghai HyMaster Technology, Co., Ltd., Shanghai 200050, China
[c] Faculty of Science and Technology, University of Twente, 7500 AE Enschede, the Netherlands

ARTICLE INFO

Keywords:
Sorption compressor
Cryocooler
Adsorption
Metal–organic frameworks
Activated carbon

ABSTRACT

Many optical devices can benefit from cryogenic cooling; however, the resolution of these devices suffers from microvibration from mechanical cryocoolers. Unlike mechanical cryocoolers, sorption cryocoolers do not have any active moving parts and are essentially vibration-free. Sorption cryocoolers are thermally driven and their performance is highly determined by the properties of the adsorbents employed in the compressors. In this study, the thermodynamic and dynamic modelling of sorption compressors adopting Saran activated carbon, MOF-5 and HKUST-1 metal–organic frameworks as adsorbents are conducted to find suitable adsorbents to realize efficient compression. It is found that a sorption compressor with MOF-5 as the adsorbent has the worst performance. Saran carbon has the highest mass-flow rate. And whether HKUST-1 or Saran carbon has higher efficiency depends on the operating conditions. The effects of heat sink temperature and heater power on the performance of sorption compressors are also investigated. The analysis method can be employed to choose suitable sorbent materials and operating conditions when designing sorption compressors.

1. Introduction

Many electronic devices could benefit from operating at cryogenic temperatures [1]. Among these cryogenic electronics, optical sensors like infrared detectors and X-ray detectors are sensitive to microvibration. Widespread use of these optical sensors requires vibration-free cryocoolers. Cryocoolers combined with mechanical compressors still induce microvibration, although active and/or passive isolation techniques have been employed [2]. By employing heat rather than mechanical work, sorption cryocoolers are attractive for cooling optical sensors because of their advantages of no oil, no vibration (except for several check valves), no electromagnetic interference, high reliability and long lifetime [3].

As a key component of a sorption cryocooler, a sorption compressor is based on alternately heating and cooling porous materials as adsorbents to realize the gas cycle of pressurization, exhaust, depressurization and suction. Sorption compressor adsorbs low-pressure gas at low temperatures, and desorbs high-pressure gas at relatively high temperatures.

According to the interaction between gas and adsorbent, sorption can be divided into physical adsorption (physisorption) and chemical absorption (chemisorption) [4]. In physisorption, the interaction between gas and adsorbent mainly depends on the electrostatic force and the Van der Waals force. Silica gel [5] and zeolite [6] were used as adsorbents in the early research of sorption compressors. However, due to the limited adsorption characteristics of these two adsorbents, research on sorption compressors had been stagnant for years. Presently, the physisorption compressors mainly use activated carbon as adsorbents [7], whereas helium-3 [8], helium-4 [9], hydrogen [10], neon [11], nitrogen [12], argon [13], oxygen [13], methane [14], krypton [15], xenon [16], ethylene [17], gas mixture of nitrogen and hydrocarbons [18] are used as working fluids. However, it is found that due to the low adsorption capacities of activated carbons at room temperature, they often need to be precooled below ambient temperature to obtain considerable adsorption capacities, which will increase the complexity of sorption compressors. In chemisorption, the electron transfer, exchange or sharing occurs between the gas and the adsorbent, forming chemical bonds. Metallic hydride [19] and praseodymium cerium oxide [20] have been used for chemisorption, which are for hydrogen and oxygen adsorption, respectively. The advantages of chemisorption materials are that they have large adsorption capacities and operate at or above ambient temperatures. However, chemisorption is only suitable for specific combination of working fluid and adsorbent, and its

* Corresponding author.
E-mail address: HaishanCao@tsinghua.edu.cn (H. Cao).

https://doi.org/10.1016/j.cryogenics.2022.103441
Received 4 October 2021; Received in revised form 22 February 2022; Accepted 23 February 2022
Available online 28 February 2022

Nomenclature

c_p	specific heat capacity at constant pressure [J kg^{-1} K^{-1}]
c_v	specific heat capacity at constant volume [J kg^{-1} K^{-1}]
D	diameter [m]
g	specific Gibbs free energy [J kg^{-1}]
h	specific enthalpy [J kg^{-1}]
L	length [m]
m	mass [kg]
$\dot{m}$	mass-flow rate [kg s^{-1}]
M	molar mass [kg mol^{-1}]
p	pressure [Pa]
q	amount of heat per unit mass of adsorbent per cycle [J kg^{-1}]
$\dot{q}_{gen}$	heat generation [W m^{-3}]
$\dot{Q}$	heat-flow rate (power) [W]
r	radius [m]
R	universal gas constant [J K^{-1} mol^{-1}]
t	time [s]
T	temperature [K]
u	specific internal energy [J kg^{-1}]
V	volume [m^3]
x	amount normalized to the adsorbent mass [kg kg^{-1}]

Greek letters

Δ	difference of two items
η	efficiency of the sorption compressor [-]
λ	thermal conductivity [W m^{-1} K^{-1}]
ϕ	porosity [-]
ρ	bulk density [kg m^{-3}]

Subscript

ads	adsorbed
cell	sorption cell
CONT	container
cyc	cycle
dy	dynamic
fre	fre gas
H	high pressure or heating temperature
heat	heating
HS	heat sink
HT	heater
input	input heat
iso	isosteric heat of adsorption
L	low pressure or cooling temperature
sen	sensible heat
sor	adsorbent
SOR	adsorbent mixture
SW	heat switch
th	thermodynamic
tot	total

Abbreviations and acronyms

CFHX	counter-flow heat exchanger
MOFs	metal–organic frameworks

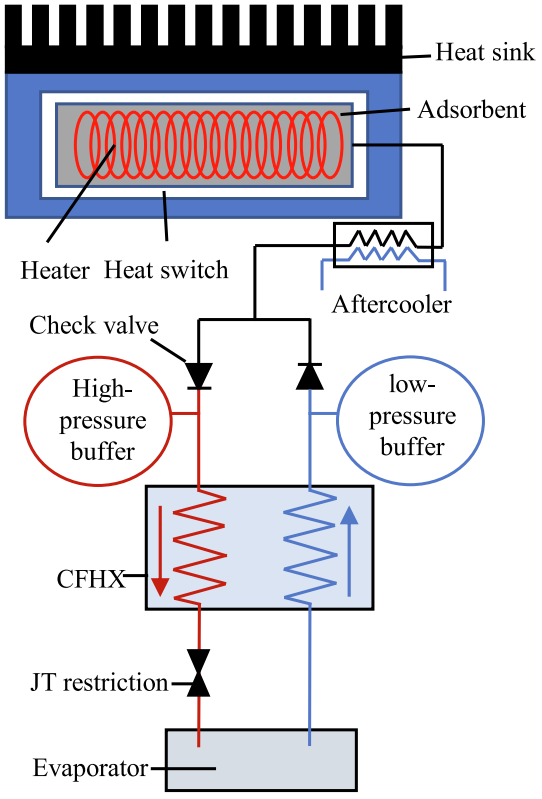

Fig. 1. Schematic of a sorption cryocooler, adapted from [26].

application ranges are narrow. Moreover, chemisorption in general also has the disadvantage of irreversibility, the material degenerates over time when cycling between adsorption and desorption.

Due to the drawbacks of the physical and chemical sorption materials, the shortage of highly efficient adsorption materials has become the bottleneck of the miniaturization of sorption compressors. In order to realize efficient and reliable miniature compressors, it is necessary to explore adsorption materials with high efficiency and stability, suitable for different working fluids and meeting the requirements of different cooling temperatures. Compared with silica gel, zeolite and activated carbon, Metal–organic frameworks (MOFs) have higher porosity, larger specific surface area and larger adsorption capacity [21]. Moreover, due to the adjustable size, shape and function of their porous structures, MOFs can achieve comprehensive properties that other materials cannot match. The application of MOFs in gas storage [22], separation [23] and catalysis [24] has been widely concerned, but the application of MOFs in sorption compressors is rarely studied [25]. This study investigates whether MOFs are applicable for sorption compressors, and the performance of sorption compressors using methane as working fluid and Saran activated carbon, MOF-5 and HKUST-1 as adsorbents is analyzed and compared. Section 2 presents the modelling of a sorption compressor, including a thermodynamic model and a dynamic model. In Section 3, the optimized efficiencies of sorption compressors with three adsorbents under different cooling temperatures, exhaust pressures and suction pressures are compared based on the thermodynamic model. The actual compressor efficiencies and mass-flow rates are analyzed based on the dynamic model in Section 4. The paper is closed with conclusions in Section 5.

2. Modelling

A basic sorption cryocooler is composed of a JT cold stage and a sorption compressor (see Fig. 1). The main components of the JT cold stage include a counter-flow heat exchanger (CFHX), a restriction and an

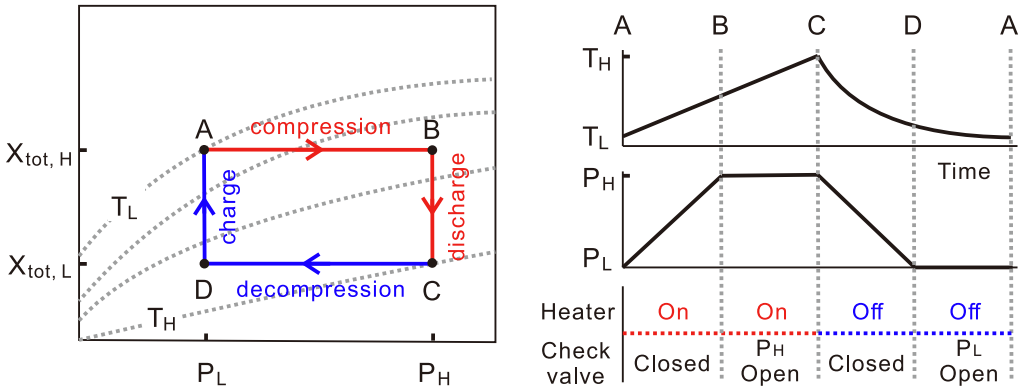

Fig. 2. Schematic of a compression cycle in the diagram with total adsorption isotherms and as a function of time.

evaporator. The sorption compressor consists of a container filled with an adsorbent equipped with a heater, a heat switch [27], a heat sink, an aftercooler, two check valves and two buffers to stabilize the suction and exhaust pressures. The high-pressure gas from the sorption compressor undergoes JT expansion when it flows through a restriction, resulting in a lower temperature. In the steady state operation, the high-pressure gas upon JT expansion produces liquid, which is contained in the evaporator. The devices mounted on the evaporator can then be cooled by evaporation of the condensed liquid. The evaporated working fluid returns through the low-pressure line of the CFHX, thereby cooling the high-pressure gas flowing in the opposite direction.

Fig. 2 schematically shows a compression cycle in the diagram with total adsorption isotherms. At the initial state point A, the sorption cell is heated. When the pressure increases to the state point B, the check valve of the high-pressure channel opens, and the gas is desorbed from the adsorbents and flows out of the sorption cell. When the temperature has increased to the state point C, heating is stopped, the heat switch turns on and the adsorbent starts to reduce in temperature. When the pressure decreases to the state point D, the check valve of the low-pressure channel opens, and the gas flows back to the sorption cell and is adsorbed on the adsorbents, thus one cycle is completed.

2.1. Thermodynamic model

From a thermodynamic point of view, the ideal performance of a sorption compressor can be estimated. The thermodynamic model is based on the following assumptions:

(1) The temperature and pressure inside the sorption cell are uniform;
(2) The aftercooler and the CFHX of the sorption cryocooler are both ideal. In other words, the high-pressure gas is cooled to the cooling temperature (T_L in Fig. 2) by passing through the aftercooler, whereas the low-pressure gas from the evaporator is heated to the cooling temperature by passing through the CFHX;
(3) Since we aim to compare the adsorbents, the heat consumed by the heater, the container and the heat switch, as well as the heat losses to the environment are neglected;
(4) In order to analyze the performance difference induced by the intrinsic properties of the adsorbent materials, the dead volume contribution due to the cell itself (e.g. tubing volume between the adsorbent and the check valves) is neglected, and only the dead volume due to the pores in the adsorbent is considered;
(5) The equilibrium time of adsorption and desorption is much shorter than that of heat transfer and fluid flow, which implies that the amount of the working fluid in the sorption cell at a particular time can be calculated based on the pressure and temperature.

The performance of a sorption compressor is evaluated by the efficiency (η_{th}) in the thermodynamic model, which is defined by the ratio of the change in Gibbs free energy of the working fluid to the input heat into the compressor [28],

$$\eta_{th} = \frac{\Delta g \Delta x_{tot}}{q_{input}} \tag{1}$$

where Δg is the difference in specific Gibbs free energy between the inflow and the outflow gas, Δx_{tot} and q_{input} are the delivery amount of working fluid and the input heat per unit mass of adsorbent per cycle, respectively.

Since both the aftercooler and the CFHX are assumed to be ideal, the temperatures of the outflow and inflow gas are both equal to the cooling temperature (T_L). As a result, the Δg can be expressed as [29]:

$$\Delta g = g(P_H, T_L) - g(P_L, T_L) \tag{2}$$

where P_L and P_H are the suction and exhaust pressures, respectively.

The Δx_{tot} is determined by the difference in the normalized total adsorption amount between the state points A and C shown in Fig. 2:

$$\Delta x_{tot} = x_{tot}|_A - x_{tot}|_C = (x_{ads} + x_{fre})|_A - (x_{ads} + x_{fre})|_C \tag{3}$$

where x_{ads} and x_{fre} are the normalized adsorbed and free gas amount, respectively. x_{ads} is calculated according to the absolute adsorption isotherms, whereas x_{fre} is given by [26],

$$x_{fre} = \rho_{fre}\left(\frac{\phi}{\rho_{sor}} - \frac{x_{ads}}{\rho_{ads}}\right) \tag{4}$$

where ρ_{fre} and ρ_{ads} are the densities of free gas and adsorbed phase, respectively. ρ_{sor} is the bulk density of the adsorbent, and ϕ is the porosity of the adsorbent.

q_{input} is determined by the integration of the input heat in an infinitesimal step (dq_{input}) over the heating process (A→B→C in Fig. 2). dq_{input} is consumed by the sensible heats for the adsorbent ($dq_{sor,sen}$), adsorbed phase ($dq_{ads,sen}$) and free gas ($dq_{fre,sen}$), and the heat of adsorption (dq_{ads}), written as,

$$dq_{input} = dq_{sor,sen} + dq_{ads,sen} + dq_{fre,sen} + dq_{ads} \tag{5}$$

The mass of the adsorbent and adsorbed phase can be regarded as constant in each small step. According to the first law of thermodynamics for a closed system [30], the sensible heats for the adsorbent and adsorbed phase are given by,

$$dq_{sor,sen} = du_{sor} \tag{6}$$

$$dq_{ads,sen} = du_{ads} \tag{7}$$

where du is the change in internal energy.

The volume changes of the adsorbent and adsorbed phase are small and their contribution to the internal energy can be neglected. Therefore, the changes in internal energy of the adsorbent and adsorbed phases can be calculated by,

$$du_{sor} = c_{v,sor}(T,p)dT \tag{8}$$

$$du_{ads} = x_{ads}(T,p)c_{v,ads}(T,p)dT \tag{9}$$

where $c_{v,sor}$ and $c_{v,ads}$ are the specific heat capacities at constant volume of the adsorbent and adsorbed phase, respectively.

The mass of free gas is assumed to be constant in a small time step during the compression phase (A→B in Fig. 2). The sensible heat for free gas during the compression phase can be calculated by,

$$dq_{fre,sen}|_{A\to B} = du_{fre} = x_{fre}(T,p)|_{A\to B}c_{v,fre}(T,p)dT \tag{10}$$

where $x_{fre}|_{A\to B}$ denotes the normalized mass of free gas in the sorption cell, calculated as Eq. 4.

In discharge phase (B→C in Fig. 2), some free gas flows out of the sorption cell with a constant exhaust pressure. If we take the gas remaining in the cell and the discharged gas as a closed system, then this system undergoes an isobaric process. The sensible heat for free gas during the discharge phase can be calculated by,

$$dq_{fre,sen}|_{B\to C} = dh_{fre} = x_{fre}(T,p)|_{B\to C}c_{p,fre}(T,p)dT \tag{11}$$

where dh_{fre} is the change in enthalpy, $c_{p,fre}$ is the specific heat capacity at constant pressure of free gas, and $x_{fre}|_{B\to C}$ is the normalized mass including both free gas in the sorption cell and the discharged gas, calculated as,

$$x_{fre}(T,p)|_{B\to C} = x_{tot}|_A - x_{ads}(T,p) \tag{12}$$

The heat of adsorption dq_{ads} is calculated by,

$$dq_{ads} = q_{iso}(T,p)\cdot[x_{ads}(T+dT,p+dp) - x_{ads}(T,p)] \tag{13}$$

where q_{iso} is the isosteric heat of adsorption, given by [31],

$$q_{iso}(T,p) = \frac{RT^2}{Mp}\left(\frac{\partial p}{\partial T}\right)_{x_{ads}} \tag{14}$$

By combining Eqs. (5)–(14), one can derive,

$$dq_{input} = c_{v,sor}(T,p)dT + x_{ads}(T,p)c_{v,ads}(T,p)dT + \begin{cases} x_{fre}(T,p)|_{A\to B}c_{v,fre}(T,p)dT \\ x_{fre}(T,p)|_{B\to C}c_{p,fre}(T,p)dT \end{cases} + \frac{RT^2}{Mp}\left(\frac{\partial p}{\partial T}\right)_{x_{ads}}\cdot[x_{ads}(T+dT,p+dp) - x_{ads}(T,p)] \tag{15}$$

As a result, q_{input} can be calculated by integrating dq_{input} along the curve $A\to B\to C$ in Fig. 2,

$$q_{input} = \int_{A\to B} dq_{input}|_{x_{tot}} + \int_{B\to C} dq_{input}|_p \tag{16}$$

It should be noted that the specific heat capacity at constant pressure was used to calculate the sensible heats of all the materials in some studies [13,28], whereas the type of specific heat capacity was not clearly specified in others [32,33]. For the adsorbent and adsorbed phase, c_p and c_v are close, whereas the sensible heat of free gas occupies a small percentage in the total input heat (less than 5% in our simulated cases). As a result, the different calculation methods for input heat do not result in significant differences in the efficiency and mass-flow rate. Despite this, the calculation method presented in this study has more clear physical meaning and is beneficial to understanding the compression process of sorption compressors.

By combining Eqs. (1)–(4) and Eq. 16, the compressor efficiency can be calculated. For a compressor with fixed suction pressure, cooling temperature and exhaust pressure, the compressor efficiency is a function of the heating temperature. And the optimized efficiency refers to the maximum efficiency, which corresponds to the optimum heating temperature. In Section 3, the optimized efficiencies of compressors using MOF-5, HKUST-1 and Saran carbon as the adsorbents are compared and analyzed based on the thermodynamic model.

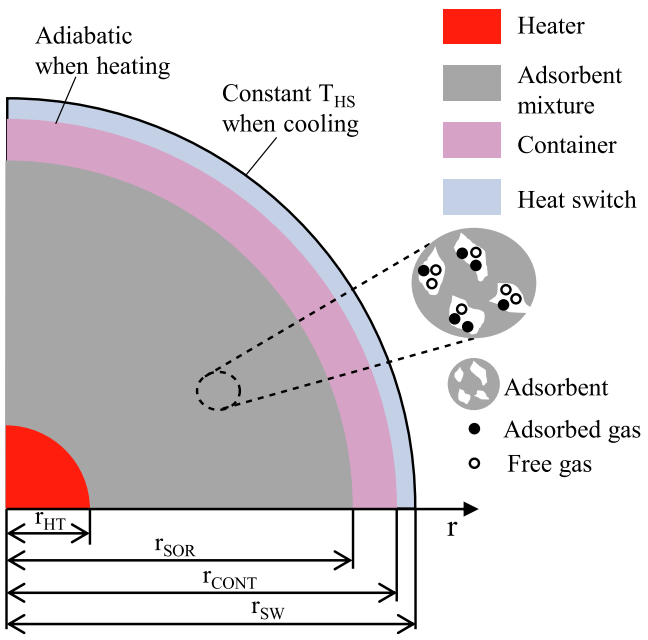

Fig. 3. Cross-section of the cylindrical sorption cell in the dynamic model.

Table 1
The radial dimensions of the compressors in the dynamic model.

r_{HT} (mm)	r_{SOR} (mm)	r_{CONT} (mm)	r_{SW} (mm)
0.5	5	5.25	5.35

Table 2
The lengths of the compressors in the dynamic model.

Adsorbent	MOF-5 [34–37]	HKUST-1 [34–36,38]	Saran [10,39]
Length (mm)	200	141	113

2.2. Dynamic model

In order to investigate the effect of the finite thermal conductivities of adsorbents on compressor performance and understand the compressor behavior in practical cycles, a dynamic model was built and implemented in MATLAB code. The model can be used to predict the dynamic performance of the sorption compressor and to optimize the compressor design. The dynamic model presented in this study is based on the configuration of the sorption cell shown in Fig. 3. The sorption cell consists of a heater, an adsorbent mixture, a cell container and a heat switch. The relative positions of the components are shown in Fig. 3. The adsorbent mixture refers to the mixture of the adsorbent, the adsorbed gas and the free gas. The dimensions of the compressors in the dynamic model are given in Tables 1 and 2. The radial dimensions of the compressors are identical for the three adsorbents, while the sorption-cell length for each adsorbent is inversely proportional to its bulk density in order to compare the compressor performance under the same total adsorbent mass condition (7.9 g in this study).

The dynamic model is based on the following assumptions:

Table 3
The heat generation terms of the components of the sorption cell.

Component	Heater	Adsorbent mixture	Cell container	Heat switch
Heat generation	$\frac{4\dot{Q}_{HT}}{\pi D_{HT}^2 L}$	$\rho_{sor}\cdot q_{iso}\frac{\partial x_{ads}}{\partial t}$	0	0

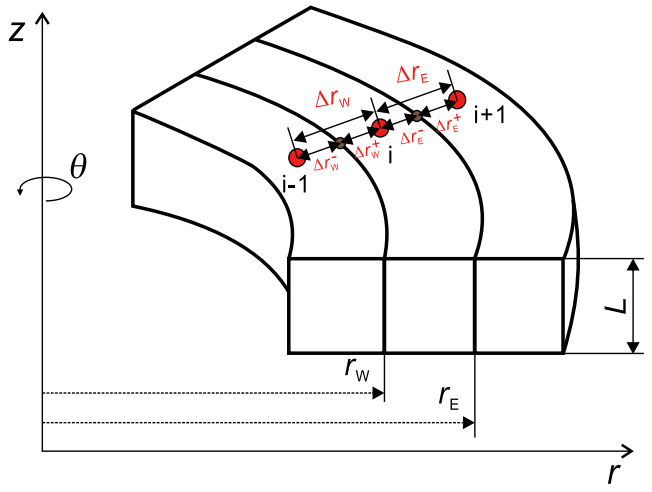

Fig. 4. Element distribution along the radius direction, adapted from [33].

(1) As a result of the cylindrical configuration and long length over diameter ratio of the sorption cell, 1-dimensional dynamic model is adopted in this study, and only the radial temperature gradient is considered;
(2) At a specific radius, the adsorbent, adsorbed gas and free gas of the adsorbent mixture have the same temperature;
(3) Due to the slow flow process in the sorption cell, the pressure drop through the adsorbent pores is neglected;
(4) The check valves are ideal, that is, the cracking pressure (pressure difference between check valve's inlet and outlet) is zero.
(5) Since OFF conductance of the heat switch is much smaller than its ON conductance, it is assumed that the heat switch has an infinite resistance at the OFF state. Therefore, the boundary condition at the cell container is adiabatic during the heating process. Whereas the thermal resistance at the ON state is calculated based on Eqs. (13)–(20) of literature [40].

In addition to the above assumptions, the dynamic model also includes assumptions 4 and 5 of the thermodynamic model.

In the dynamic model, the general energy conservation equations for the components of the sorption cell can be expressed by:

$$\begin{cases} \rho c_v \dfrac{\partial T}{\partial t} = \nabla\cdot(\lambda\nabla T) + \dot{q}_{gen} & \text{compression/decompression phase} \\ \rho c_p \dfrac{\partial T}{\partial t} = \nabla\cdot(\lambda\nabla T) + \dot{q}_{gen} & \text{discharge/charge phase} \end{cases} \tag{17}$$

The heat generation terms ($\dot{q}_{gen}$) for the components of the sorption cell are given in Table 3, where $\dot{Q}_{HT}$ is the heating power of the heater, D_{HT} is the heater diameter and L is the heater length (i.e. the sorption cell length).

In compression and decompression phases, the pressure inside the cell can be calculated by the conservation of the total mass of the adsorbed and free gases, while the pressures in discharge and charge phases are constant set by the check valves. That is:

$$\begin{cases} \dfrac{d\left(\iiint_{V_{cell}} dx_{tot}(P,T)\right)}{dt} = 0 & \text{compression/decompression phase} \\ p(t) = p_H & \text{discharge phase} \\ p(t) = p_L & \text{charge phase} \end{cases} \tag{18}$$

There are two equations for each phase (Eqs. 17 and 18) and four unknowns: T, p, x_{ads} and x_{fre}. Therefore, two more equations are required to close the equations, which are the adsorption isotherm equation $x_{ads} = f_1(p,T)$ and the real gas equation of state $\rho = f_2(p,T)$. In this study, the adsorption isotherms are calculated based on the data from [34,39]. And the density of free gas is derived from REFPROP according to the Helmholtz equation of state for methane [41,42].

As shown in Fig. 4, for a control volume of one radian, the 1-dimensional energy conservation equation (Eq. 17) is discretized according to the implicit finite control volume method [43].

$$\frac{(\rho c)_i^n (T_i^{n+1} - T_i^n)\Delta V_i}{\Delta t} = \lambda_w \cdot \frac{(T_{i-1}^{n+1} - T_i^{n+1})}{\Delta r_W} \cdot r_W L + \lambda_E \cdot \frac{(T_{i+1}^{n+1} - T_i^{n+1})}{\Delta r_E} \cdot r_E L + \dot{q}_{gen}\Delta V_i \tag{19}$$

where c stands for c_p or c_v. n and i are the indexes of time step and element, respectively. ΔV_i is the control volume of i element, given by,

$$\Delta V_i = \frac{r_E^2 - r_W^2}{2} L \tag{20}$$

As the thermal conductivity is temperature-dependent, λ_W and λ_E are the harmonic mean values between two neighbor elements [43],

$$\lambda_W = \frac{1}{\frac{1}{\lambda(T_{i-1}^n)}\frac{\Delta r_W^-}{\Delta r_W} + \frac{1}{\lambda(T_i^n)}\frac{\Delta r_W^+}{\Delta r_W}} \tag{21}$$

$$\lambda_E = \frac{1}{\frac{1}{\lambda(T_i^n)}\frac{\Delta r_E^-}{\Delta r_E} + \frac{1}{\lambda(T_{i+1}^n)}\frac{\Delta r_E^+}{\Delta r_E}} \tag{22}$$

Through this discretization, the partial differential equations of energy conservation become nonlinear algebraic equations and can be solved by MATLAB.

In the dynamic model, the efficiency is calculated by,

$$\eta_{dy} = \frac{\Delta m_{fre}\Delta g}{\dot{Q}_{HT} t_{heat}} \tag{23}$$

where Δm_{fre} is the mass of discharged gas, t_{heat} is the heating duration.

And the mass-flow rate is calculated by,

$$\dot{m} = \frac{\Delta m_{fre}}{t_{cyc}} \tag{24}$$

where t_{cyc} is the cycle time.

To verify the dynamic model, the modelling results of the dynamic model are compared to the simulated and measured data of the literature [32]. In the case given in the literature, the sorption cell using Saran carbon as the adsorbent and helium gas as the working fluid was cycled between 9.2 bar and 14.5 bar. Fig. 5 shows how the pressure and mass-flow rate change with time as the heater is switched on with a heater power of 30 W lasting for 12 s, and then the sorption cell is cooled down by liquid nitrogen for 78 s. As shown in Fig. 5, there are four main deviations between our simulated results and measured data of the literature, which are:

(1) Measured pressure is higher than the set value of the high-pressure check valve during the discharge phase, whereas it is lower than the set value of the low-pressure check valve during the charge phase (see Zoom-In A and Zoom-In B Fig. 5(a)).

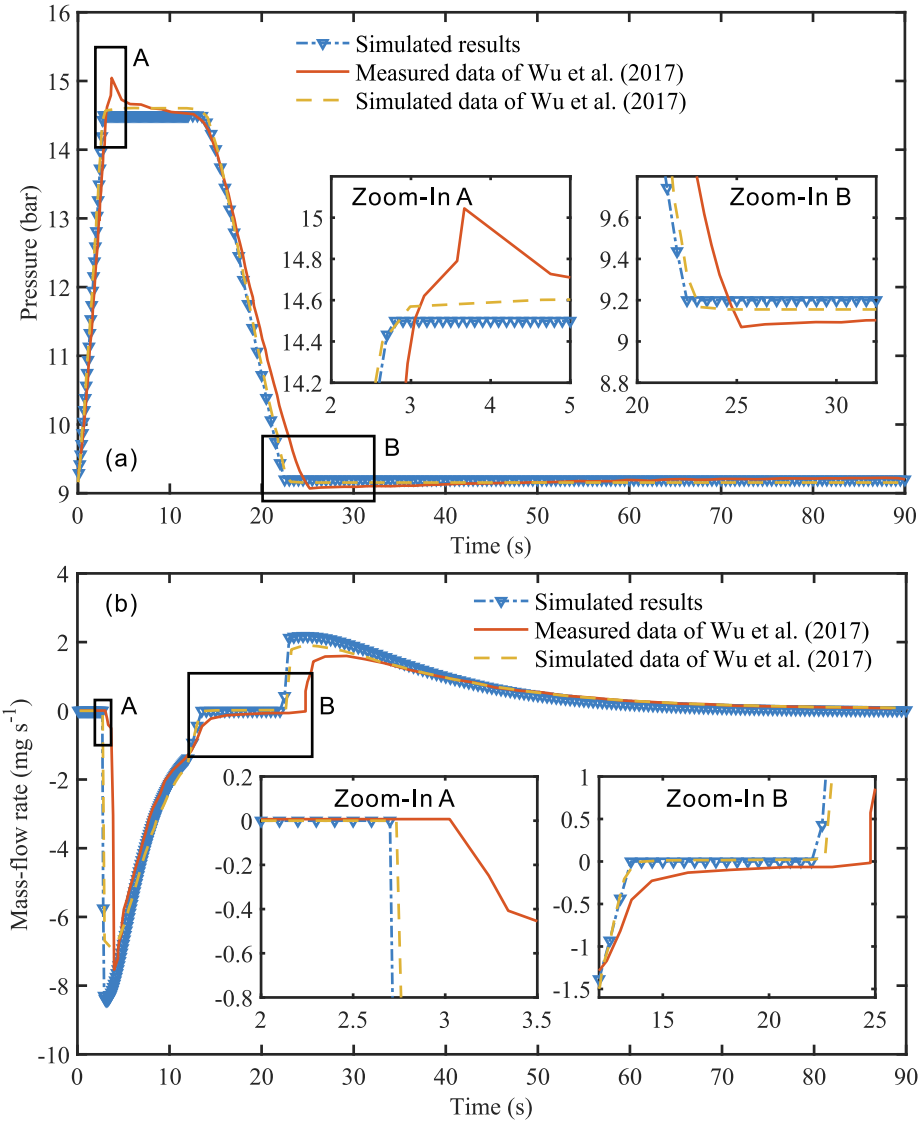

Fig. 5. (a) Predicted pressure and (b) mass-flow rate compared to the simulated and measured data of the literature [32]. The sorption cell filled with helium was initially heated with a heater power of 30 W lasting for 12 s, followed by cooling with liquid nitrogen for 78 s. The negative and positive mass-flow rates refer to the mass-flow rates of the discharge and charge phases, respectively.

(2) Simulated pressure reaches the exhaust/suction pressure faster than measured pressure (see Zoom-In A and Zoom-In B Fig. 5(a)). Correspondingly, simulated discharge and charge phases both start earlier than measured results (see Zoom-In A and Zoom-In B Fig. 5(b)).
(3) Measured out-flow has a small non-zero value at the end of the discharge phase (see Zoom-In B Fig. 5(b)).
(4) Simulated peak values of out-flow and in-flow are both higher than the measurement.

These deviations can be mainly attributed to reasons from two aspects.

The first reason is the non-ideality of the valves, which is not taken into account in the dynamic model. Due to the cracking pressure of the check valves, the measured pressure is higher than the set exhaust pressure during out-flow and lower than the set suction pressure during in-flow. In addition, the cracking pressure of the check valves also contributes to earlier start times of the simulated discharge and charge phases. Furthermore, the check valve cannot close immediately, leading to a small measured mass-flow rate at the end of the discharge phase.

The second reason is the uncertainty of the properties of the adsorbent and the adsorption isotherms. An increase in the specific heat capacity of the adsorbent results in a decline in the change rate of the average adsorbent temperature and the pressure inside the cell, and thus the delayed start times of the discharge and charge phases. Meanwhile, the peak values of out-flow and in-flow decrease with increasing specific heat capacity. When the thermal conductivity of the adsorbent decreases, the time that the pressure inside the cell reaches the exhaust/suction pressure increases, so do the start times of the discharge and charge phases. Whereas the peak values of out-flow and in-flow decrease. This can be explained in such a way that a smaller thermal conductivity of the adsorbent results in a larger temperature gradient in the sorption cell. In other words, the inner adsorbent is over-heated whereas the outer adsorbent is not heated sufficiently. In addition, a decrease in the adsorption amount also leads to a lowered change rate of pressure and reduced peak values of out-flow and in-flow.

To summarize, the integration of non-ideality of the valves, underestimated specific heat capacity of the adsorbent, as well as overestimated thermal conductivity of the adsorbent and adsorption amount is possibly the main reason that leads to the deviation between simulated and measured results. Due to the deviation, reasonable margins should be considered using this dynamic model to design a sorption

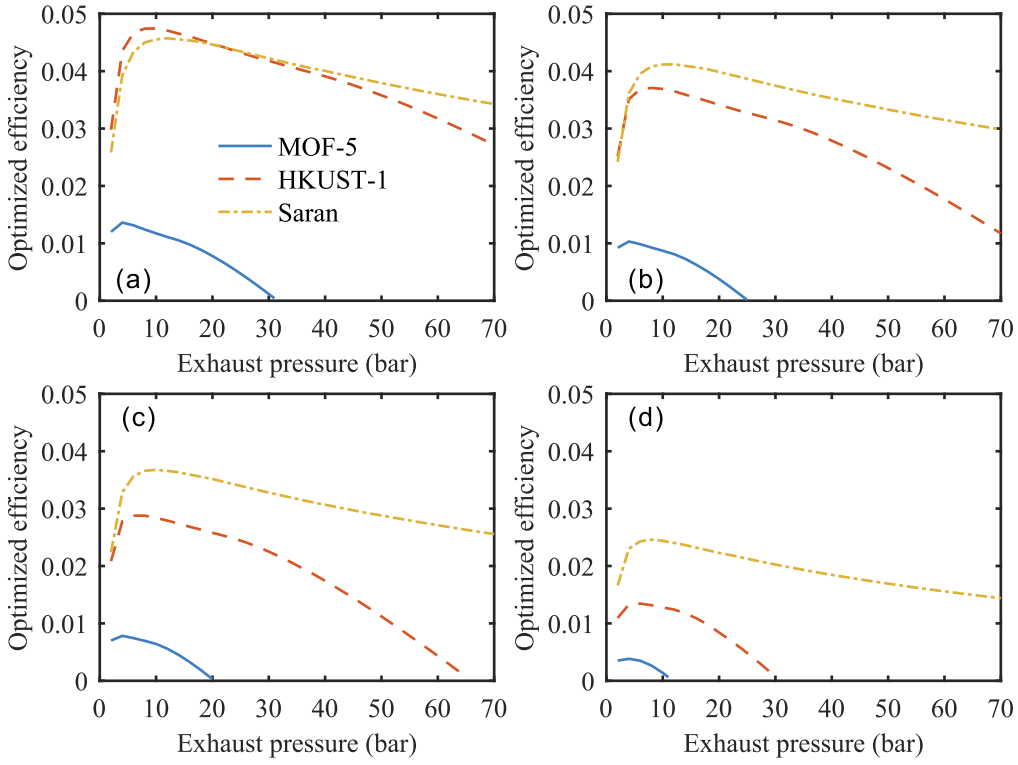

Fig. 6. Optimized efficiency as a function of the exhaust pressure for the three adsorbents at a given cooling temperature of 250 K (a), 260 K (b), 270 K (c) and 300 K (d). The suction pressure is fixed at 1 bar.

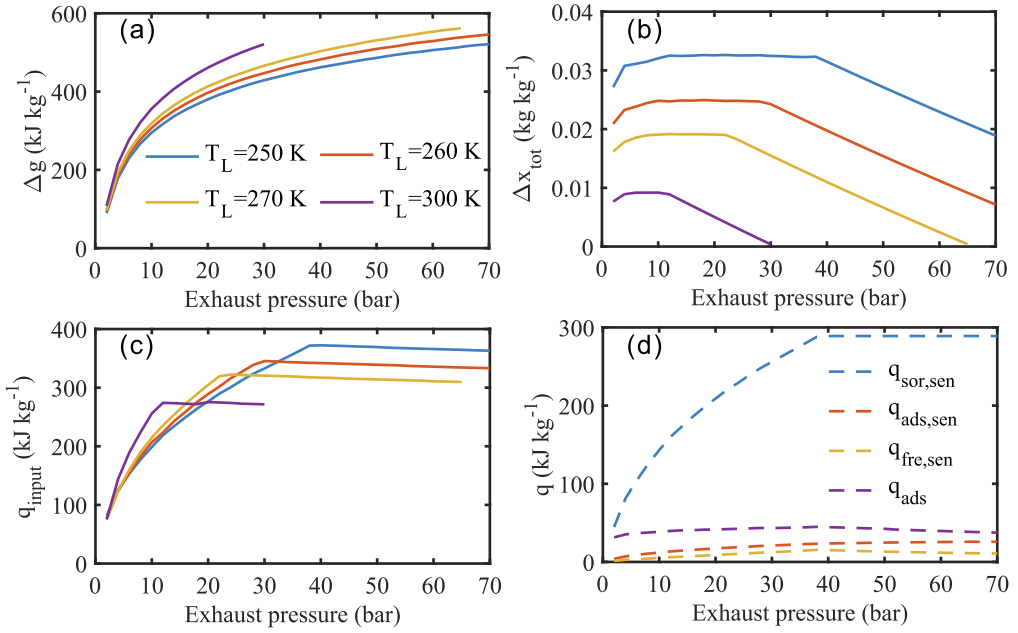

Fig. 7. (a) Difference in specific Gibbs free energy (Δg), (b) delivery amount of methane (Δx_{tot}), (c) total input heat (q_{input}) and (d) energy consumption of each item per cycle for $T_L = 250$ K as a function of the exhaust pressure for HKUST-1. The suction pressure is fixed at 1 bar.

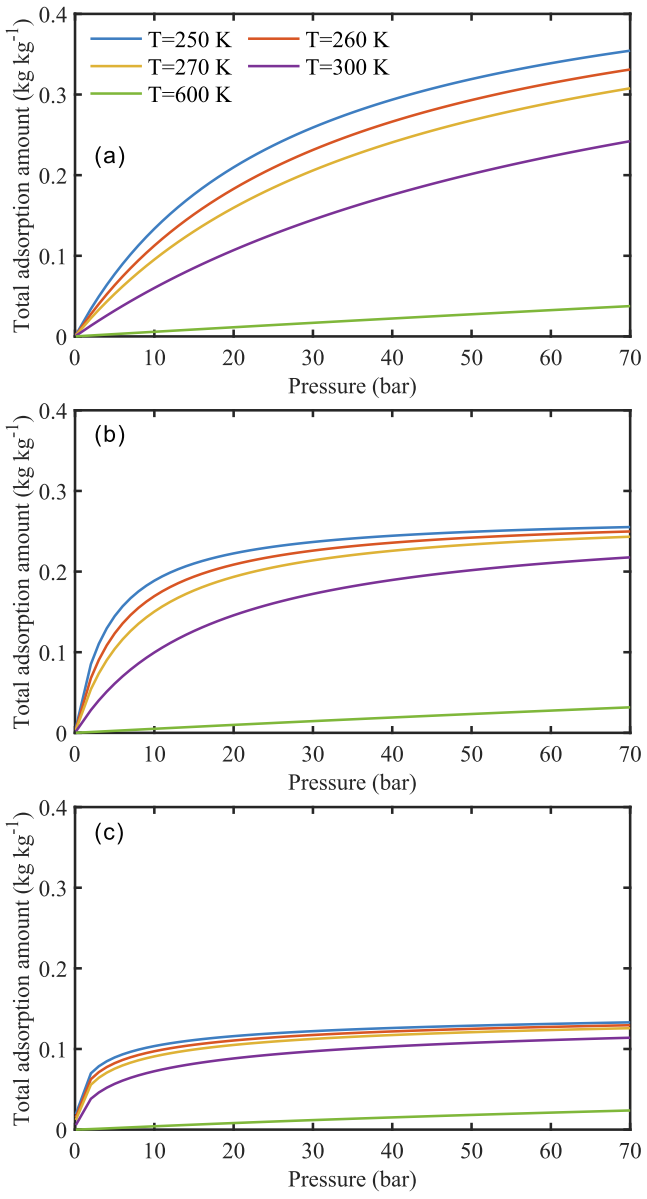

Fig. 8. Total adsorption isotherms of methane on MOF-5 (a), HKUST-1 (b) and Saran (c) [34,39].

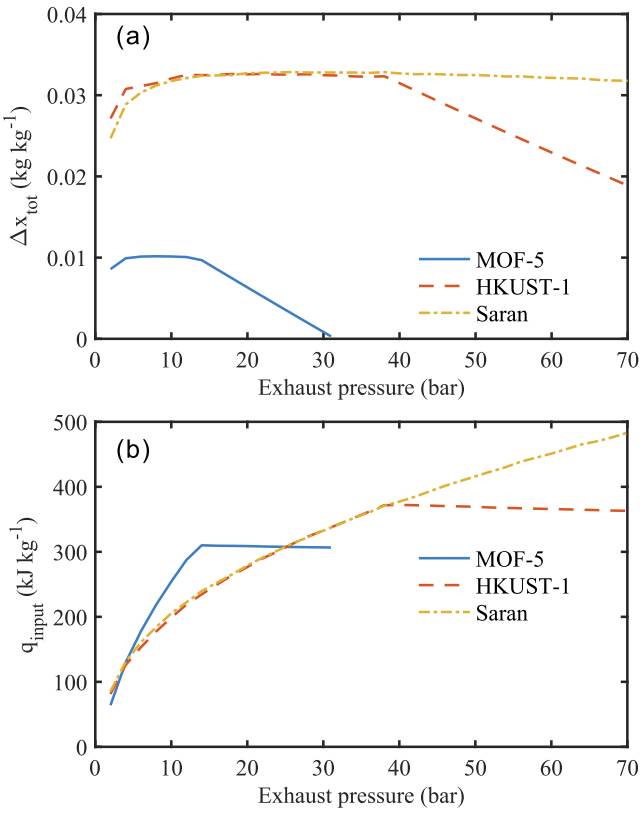

Fig. 9. (a) The delivery amount of methane (Δx_{tot}); (b) total input heat (q_{input}) per cycle for $T_L = 250$ K as a function of the exhaust pressure for the three adsorbents. The suction pressure is fixed at 1 bar.

compressor. In this study, we focus on the performance comparison of the three adsorbents, and the deviation is deemed to be acceptable.

3. Thermodynamic analysis

3.1. Effect of the exhaust pressure

Fig. 6 shows a comparison of the optimized compressor efficiency among the three adsorbents. The optimized efficiency is plotted as a function of exhaust pressure at different cooling temperatures. It is important to realize that the highest heating temperatures for MOF-5 and HKUST-1 are limited to their decomposition temperatures, which are generally measured as 623 K for both adsorbents [44,45]. Therefore, the heating temperature limit is set at 600 K for these two adsorbents in both the thermodynamic and dynamic models, whereas there is no such limit for Saran carbon. For a given adsorbent (taking HKUST-1 as an example), the optimized efficiency increases with decreasing cooling temperature for a given exhaust pressure, and increases at first and then decreases with increasing exhaust pressure for a given cooling temperature.

The changes of efficiency are caused by multiple factors including the delivery amount, the specific Gibbs free energy and the input heat as shown in Fig. 7. The difference in specific Gibbs free energy between the inflow and the outflow gas increases with increasing cooling temperature and exhaust pressure. The delivery amount of methane of a cycle, which is determined by the total adsorption isotherms (see Fig. 8), increases with the decrease in the cooling temperature for a given exhaust pressure. However, the delivery amount of methane of a cycle does not change monotonically with exhaust pressure for a given cooling temperature because of the inconsistent optimum heating temperatures for different exhaust pressures (see Fig. 7(b)).For a given cooling temperature, the input heat first increases with increasing exhaust pressure and then slightly decreases after the optimal heating temperature reaches 600 K. And how the input heat changes with the cooling temperature depends on the exhaust pressure. The input heat is mainly consumed by four items, including the sensible heats of the free phase, adsorbed phase and adsorbent, and the heat of adsorption, among which the sensible heat of adsorbent accounts for the largest proportion. This indicates that the specific heat capacity of the adsorbent should be as small as possible in order to improve the optimized efficiency of the compressor. The sensible heat of adsorbent first increases and then keeps constant as the exhaust pressure achieves 40 bar. The reason is that the optimum heating temperature corresponding to the optimized efficiency for a given exhaust pressure first increases with increasing exhaust pressure and then reaches the temperature limit of 600 K at 40 bar.

As shown in Fig. 6, when the cooling temperature is 250 K and the exhaust pressure is less than 22 bar, HKUST-1 has the highest optimized efficiency, followed by Saran carbon and MOF-5 in turn. However, as the exhaust pressure exceeds 22 bar or the cooling temperature exceeds 260 K, Saran carbon has the highest optimized efficiency, followed by HKUST-1 and MOF-5 in turn. Moreover, for the case with a cooling

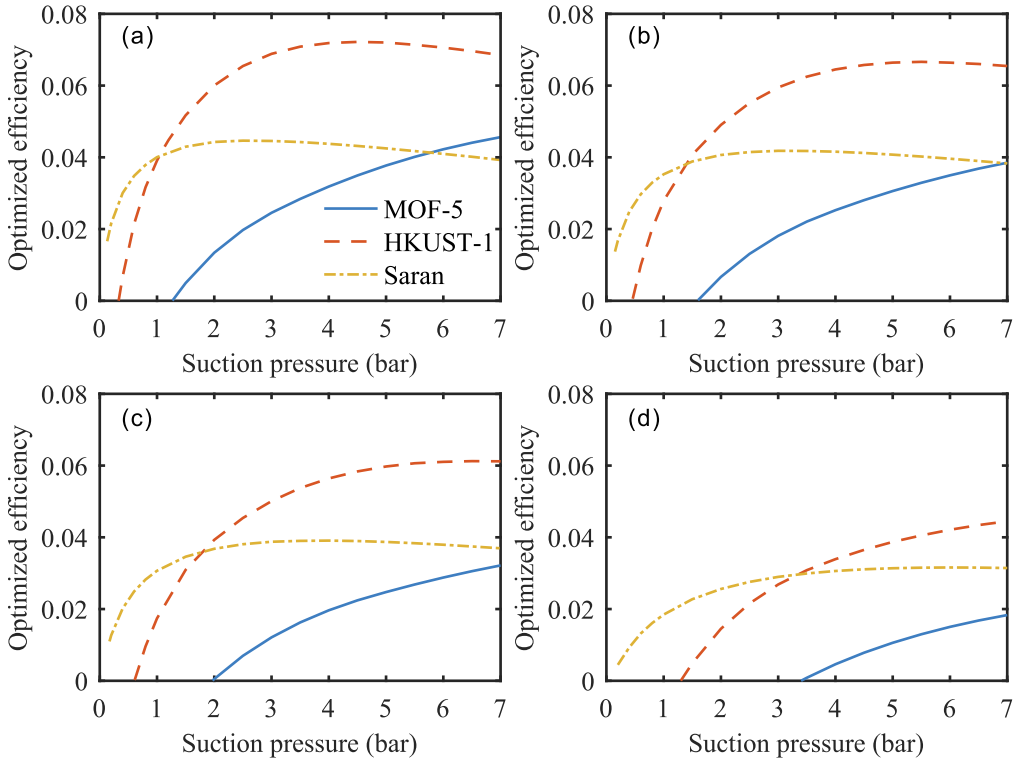

Fig. 10. Optimized efficiency as a function of the suction pressure for the three adsorbents at a given cooling temperature of 250 K (a), 260 K (b), 270 K (c) and 300 K (d). The exhaust pressure is fixed at 40 bar.

temperature of 300 K, the highest pressures that compressors based on MOF-5 and HKUST-1 can provide are only 11 bar and 30 bar, much less than the exhaust pressure of Saran based compressor. As shown in Fig. 9, the poor performance of MOF-5 based sorption compressor is mainly due to its small delivery amount of methane, followed by the large input heat per cycle. The delivery amounts of methane for HKUST-1 and Saran are relatively close when the exhaust pressure is less than about 38 bar. However, the optimal heating temperature of HKUST-1 is limited to its decomposition temperature (600 K in this study) when the exhaust pressure exceeds 38 bar. As a result, the delivery amount of methane for HKUST-1 decreases significantly with the increase of exhaust pressure, leading to lower optimized efficiency than Saran.

3.2. *Effect of suction pressure*

Fig. 10 shows optimized efficiency as a function of the suction pressure for the three adsorbents. The optimum adsorbent for a given exhaust pressure of 40 bar is determined by both the cooling temperature and the suction pressure. Saran carbon has the highest optimized efficiency when suction pressure is less than 1 bar and the cooling temperature is 250 K, which can be mainly attributed to its highest adsorption amount of methane under these conditions (see Fig. 8). As the suction pressure increases further, the optimized efficiency for HKUST-1 becomes the highest. The optimized efficiencies for Saran carbon and HKUST-1 with cooling temperatures of 250 K and 260 K first increase with increasing suction pressure, peak at certain pressures and then reduce. These trends are integrated results of the delivery amount of methane, the total input heat and the Gibbs free energy between the charge and discharge states as discussed in the Section 3.1. Although the optimized efficiencies for the two adsorbents have the same trends, the optimized efficiency peaks and corresponding suction pressures are different. As shown in Fig. 8, the temperature dependent adsorption amounts of methane on Saran carbon flatten out at lower pressures. This explains why the optimized efficiency peaks for Saran carbon occur at lower pressures than HKUST-1. In the considered suction pressure range of 0.13 bar to 7 bar, the optimized efficiencies for MOF-5 and HKUST-1 with cooling temperatures of 270 K and 300 K increase monotonically with suction pressure. That is mainly because the adsorption amount of methane on MOF-5 and HKUST-1 increase almost linearly with suction pressure in the considered range.

4. Dynamic analysis

The dynamic model is based on the sorption cell configuration that is schematically shown in Fig. 3, where the heater is at the center of the cell. In the model, the sorption cell filled with methane was initially at uniform suction pressure and cooling temperature, then the cell is heated till the temperature of the innermost layer of the adsorbent mixture reaches 600 K, followed by cooling via the heat sink till the total adsorption amount of methane returns to the initial value, which corresponds to the total adsorption amount of methane at 250 K and 1 bar. The actual efficiencies calculated using the dynamic model are compared with those calculated through thermodynamic model. Fig. 11 (a) shows that the actual efficiencies based on dynamic models are smaller than those based on thermodynamic models. The difference is mainly caused by the temperature gradient along radial direction. Fig. 11 (b) shows that when the innermost layer is heated to 600 K, the adsorbent along the radial direction is not heated sufficiently, resulting in the lower actual efficiency. It is noteworthy that the actual efficiency for HKUST-1 is lower than that for Saran carbon when the exhaust pressure is larger than about 21 bar. Fig. 11 (c) shows the mass-flow rate as a function of the exhaust pressure for the three adsorbents. The mass-flow rate decreases with the increasing exhaust pressure. Among the three adsorbents, Saran has the highest mass-flow rate.

Taking HKUST-1 as an example, the effects of heat sink temperature and heater power on the efficiency and mass-flow rate are shown in Fig. 12. Under given heater power of 10 W, the mass-flow rate increases with decreasing heat sink temperature due to the reduced cooling time

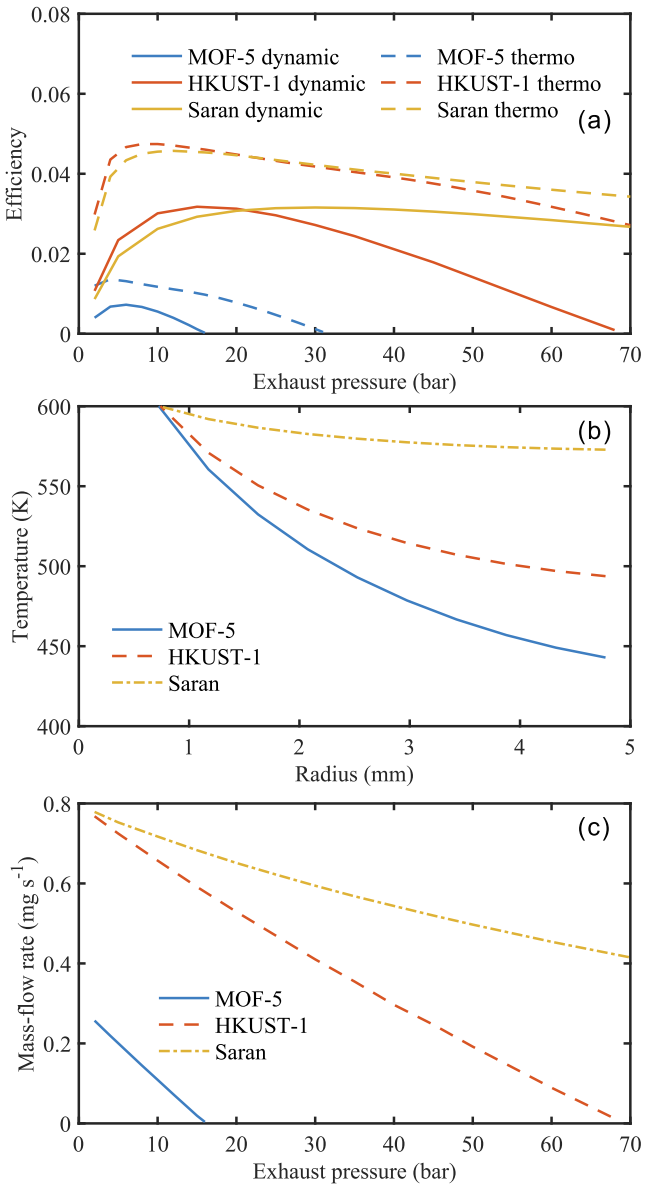

Fig. 11. (a) Actual efficiency compared to optimized efficiency as a function of the exhaust pressure for the three adsorbents; (b) temperature profile along the radial direction at the moment when the temperature of innermost layer of adsorbent mixture reaches 600 K for the case with an exhaust pressure of 15 bar; (c) mass-flow as a function of the exhaust pressure for the three adsorbents. The suction pressure, the heat sink temperature, the average cooling temperature, the highest heating temperature and the heater power are fixed at 1 bar, 245 K, 250 K, 600 K and 10 W, respectively.

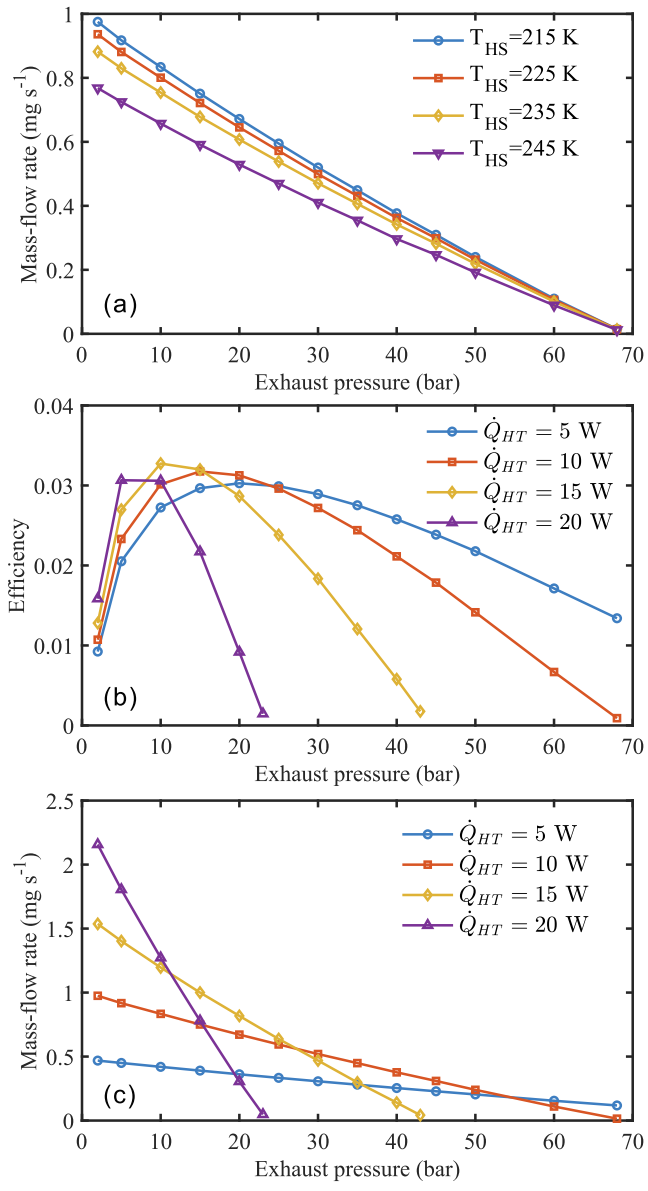

Fig. 12. (a) Mass-flow as a function of the exhaust pressure for different heat sink temperatures; (b) efficiency and (c) mass-flow as a function of the exhaust pressure for different heater powers. HKUST-1 is employed as the adsorbent. The suction pressure, the average cooling temperature and the highest heating temperature are fixed at 1 bar, 250 K and 600 K, respectively. The heater power is fixed at 10 W for (a) and the heat sink temperature is fixed at 215 K for (b) and (c).

(see Fig. 12 (a)). However, the heat sink temperature has no effect on the efficiency since the average cooling temperature is fixed at 250 K. Under given heat sink temperature of 215 K, the efficiency and mass-flow rate both have corresponding optimal heater powers, which are different from each other and both depend on the exhaust pressure.

The dynamic analysis results indicate that heat transfer enhancement measures should be taken to improve the performance of sorption compressors, such as increasing the thermal conductivity of existing adsorbents by mixing with other materials with high thermal conductivity [46], developing new adsorbents with better overall properties (larger delivery amount, smaller specific heat capacity and higher thermal conductivity), optimizing the sorption cell structure (for instance, thin-plate type sorption cell [9]) among others.

5. Conclusion

In this study, the efficiency and mass-flow rate of sorption compressors, which adopt methane as working fluid and Saran carbon, MOF-5 and HKUST-1 as adsorbents, are compared and analyzed based on thermodynamic and dynamic models. It is found that despite the total adsorption amount of methane on MOF-5 and HKUST-1 are both larger than that on Saran carbon at relatively high pressure, MOF-5 based sorption compressor has worst performance in the scope as we concerned, which can be mainly attributed to its small delivery amount of working fluid and thermal conductivity. Saran carbon has the highest mass-flow rate. And whether HKUST-1 or Saran carbon has higher efficiency depends on the operating conditions. The effects of heat sink temperature and heater power on the performance of sorption compressors are also investigated under identical suction pressure and

cooling temperature. It is concluded that the mass-flow rate increases with decreasing heat sink temperature. The optimal heater power for the efficiency differs from that for mass-flow rate. It is hoped that this study will provide a theoretical basis for more in depth studies relating to adsorbent selection for sorption compressors and optimization of operating conditions.

CRediT authorship contribution statement

Lingxiao Qin: Methodology, Software, Writing – original draft, Writing – review & editing. **Haishan Cao:** Conceptualization, Methodology, Software, Writing – review & editing, Supervision, Project administration, Funding acquisition. **Junming Li:** Methodology, Writing – review & editing, Supervision. **Yingzhe Wu:** Methodology, Software, Writing – review & editing. **Marcel ter Brake:** Methodology, Writing – review & editing, Supervision.

Declaration of Competing Interest

The authors declare that they have no known competing financial interests or personal relationships that could have appeared to influence the work reported in this paper.

Acknowledgments

This work was supported by National Natural Science Foundation of China (Grant No. U21A20494 and 52076115).

References

[1] Cao HS, ter Brake HJM. Progress in and outlook for cryogenic microcooling. Phys Rev Appl 2020;14(4):044044.
[2] Bhatt JH, Barve JJ. Control of spaceborne linear cryocoolers: A review. Prog Aerosp Sci 2019;109:100544.
[3] Doornink DJ, Burger JF, ter Brake HJM. Sorption cooling: A valid extension to passive cooling. Cryogenics 2008;48(5):274–9.
[4] Jones JA. Sorption refrigeration research at JPL/NASA. Heat Recovery Syst CHP 1993;13(4):363–71.
[5] Webb JE. Intermittent type silica gel adsorption refrigerator, 1966. US3270512A.
[6] Hartwig WH. Cryogenic refrigeration concepts utilizing adsorption pumping in zeolites. Adv Cryog Eng 1978;23:438–47.
[7] Benthem B, Doornink J, Boom E, Holland HJ, Lerou PPPM, Burger JF, ter Brake HJM. Present status of developments in physical sorption cooling for space applications. Cryogenics 2014;64:220–7.
[8] Burger JF, ter Brake HJM, Holland HJ, Meijer RJ, Veenstra TT, Venhorst GCF, Lozano-Castello D, Coesel M, Sirbi A. Long-life vibration-free 4.5 K sorption cooler for space applications. Rev Sci Instrum 2007;78(6):065102.
[9] Bae J, Kwon D, Jeong S. Development of switchless thin-plate type sorption compressor cell for 5 K sorption J-T refrigerator. Cryogenics 2020;109:103112.
[10] Wu Y, Zalewski DR, Vermeer CH, ter Brake HJM. Optimization of the working fluid for a sorption-based Joule-Thomson cooler. Cryogenics 2013;58:5–13.
[11] Wu Y, Zalewski DR, Vermeer CH, Holland HJ, Benthem B, ter Brake HJM. Baseline design of a sorption-based Joule-Thomson cooler chain for the METIS instrument in the E-ELT. Cryogenics 2017;84:37–52.
[12] Hamersztein A, Tzabar N. A dynamic model of multi-stage sorption compressors. Int J Refrig 2021;124:105–13.
[13] Luo BJ, Wang ZL, Yan T, Hong GT, Li YL, Liang JT. Theoretical study of effect of working fluid on the performance of 77–100 K adsorption cryocooler. Energy Convers Manage 2015;89:919–24.
[14] Wade L, Ryba E, Weston C, Alvarez J. Test performance of a 2 W, 137 K sorption refrigerator. Cryogenics 1992;32:122–6.
[15] Alvarez JA, Krylo RJ, Snapp RD, Weston C, Sywulka P, Abell GC. Development of an advanced sorption compressor and its application in a 125 K cryocooler. Cryocoolers 1995;8:569–79.
[16] Wiegerinck GFM, Burger JF, Holland HJ, Hondebrink E, ter Brake HJM, Rogalla H. A sorption compressor with a single sorber bed for use with a Linde-Hampson cold stage. Cryogenics 2006;46(1):9–20.
[17] Burger JF, Holland HJ, Seppenwoolde JH, Berenschot E, ter Brake HJM, Gardeniers JGE, Elwenspoek M, Rogalla H. 165 K microcooler operating with a sorption compressor and a micromachined cold stage. Cryocoolers 2002;11:551–60.
[18] Tzabar N, ter Brake HJM. Analysis of ideal sorption compressor cycles operating with gas mixtures. Adsorption 2018;24(3):325–32.
[19] Morgante G, Pearson D, Melot F, Stassi P, Terenzi L, Wilson P, Hernandez B, Wade L, Gregorio A, Bersanelli M, Butler C, Mandolesi N. Cryogenic characterization of the Planck sorption cooler system flight model. J Instrum 2009;4(12). T12016–T12016.
[20] Bard S, Jones JA, Schember HR. A two-stage 80 K/140 K sorption cryocooler. In: Scurlock RG, Bailey CA, editors, Proceedings of the Twelfth International Cryogenic Engineering Conference Southampton, UK, 12–15 July 1988, Butterworth-Heinemann, 1988. p. 626–30.
[21] Furukawa H, Cordova KE, O'Keeffe M, Yaghi OM. The chemistry and applications of metal-organic frameworks. Science 2013;341(6149):1230444.
[22] Rosi NL, Eckert J, Eddaoudi M, Vodak DT, Kim J, O'Keeffe M, Yaghi OM. Hydrogen storage in microporous metal-organic frameworks. Science 2003;300(5622):1127–9.
[23] Britt D, Furukawa H, Wang B, Glover TG, Yaghi OM. Highly efficient separation of carbon dioxide by a metal-organic framework replete with open metal sites. Proc Nat Acad Sci 2009;106(49):20637–40.
[24] Valvekens P, Vermoortele F, De Vos D. Metal-organic frameworks as catalysts: the role of metal active sites. Catal Sci Technol 2013;3(6):1435–45.
[25] Barreto J, Martins D, Branco MBC, Ribeiro RPPL, Esteves IAAC, Mota JPB, Branco JB, Gonçalves AP, Tirolien T, Bonfait G. 80 K vibration-free cooler for potential future Earth observation missions. IOP Conf Series: Mater Sci Eng 2020;755:012016.
[26] Wu R. Development of a Sorption-based Joule-Thomson Cooler for the METIS Instrument on E-ELT. PhD thesis, University of Twente, 2015.
[27] DiPirro MJ, Shirron PJ. Heat switches for ADRs. Cryogenics 2014;62:172–6.
[28] Wiegerinck GFM, ter Brake HJM, Burger JF, Holland HJ, Rogalla H. Thermodynamic optimization of sorption-based Joule-Thomson coolers. Cryogenics 2007;47(3):143–52.
[29] Burger JF. Cryogenic Microcooling, A micromachined cold stage operating with a sorption compressor in a vapor compression cycle. PhD thesis, University of Twente, 2001.
[30] Bejan A. Advanced Engineering Thermodynamics. Hoboken, New Jersey: John Wiley & Sons Inc.; 2016.
[31] Rouquerol F, Rouquerol J, Sing KSW, Llewellyn PL, Maurin G. Adsorption by Powders and Porous Solids: Principles. Methodology and Applications: Academic Press; 2014.
[32] Wu Y, Mulder T, Vermeer CH, Holland HJ, ter Brake HJM. A 1-dimensional dynamic model for a sorption-compressor cell. Int J Heat Mass Transf 2017;107:213–24.
[33] Davidesko A, Tzabar N. A numerical study on the design of sorption cells for multistage compressors. Cryogenics 2020;108:103074.
[34] Mason JA, Veenstra M, Long JR. Evaluating metal-organic frameworks for natural gas storage. Chem Sci 2014;5(1):32–51.
[35] Kloutse FA, Zacharia R, Cossement D, Chahine R. Specific heat capacities of MOF-5, Cu-BTC, Fe-BTC, MOF-177 and MIL-53 (Al) over wide temperature ranges: Measurements and application of empirical group contribution method. Microporous Mesoporous Mater 2015;217:1–5.
[36] Mu B, Walton KS. Thermal analysis and heat capacity study of metal-organic frameworks. J Phys Chem C 2011;115(46):22748–54.
[37] Purewal JJ, Liu D, Yang J, Sudik A, Siegel DJ, Maurer S, Muller U. Increased volumetric hydrogen uptake of MOF-5 by powder densification. Int J Hydrogen Energy 2012;37(3):2723–7.
[38] Huang J, Xia XX, Hu XJ, Li S, Liu K. A general method for measuring the thermal conductivity of MOF crystals. Int J Heat Mass Transf 2019;138:11–6.
[39] Data supplied by University of Twente.
[40] Burger JF, Holland HJ, van Egmond H, Elwenspoek M, ter Brake HJM, Rogalla H. Fast gas-gap heat switch for a microcooler. Cryocoolers 1999;10:565–74.
[41] Setzmann U, Wagner W. A New Equation of State and Tables of Thermodynamic Properties for Methane Covering the Range from the Melting Line to 625-K at Pressures up to 1000-Mpa. J Phys Chem Ref Data 1991;20(6):1061–155.
[42] Lemmon EW, Huber ML, McLinden MO. NIST Standard ReferenceDatabase 23: Reference Fluid Thermodynamic and Transport Properties-REFPROP, Version 9.0, 2010.
[43] Patankar SV. Numerical Heat Transfer and Fluid Flow. New York: Taylor & Francis Group; 1980.
[44] Wang S, Xie XF, Xia WK, Cui JM, Zhang SQ, Du XY. Study on the structure activity relationship of the crystal MOF-5 synthesis, thermal stability and N_2 adsorption property. High Temp Mater Processes (London) 2020;39:171–7.
[45] Xavier M. Development of a system for adsorption measurements in the 77-500 K and 1-100 bar range. Master's thesis, Universidade Nova de Lisboa, 2016.
[46] Liu D, Purewal JJ, Yang J, Sudik A, Maurer S, Mueller U, Ni J, Siegel DJ. MOF-5 composites exhibiting improved thermal conductivity. Int J Hydrogen Energy 2012;37(7):6109–17.